Spin Frustration and the Kagomé Lattice

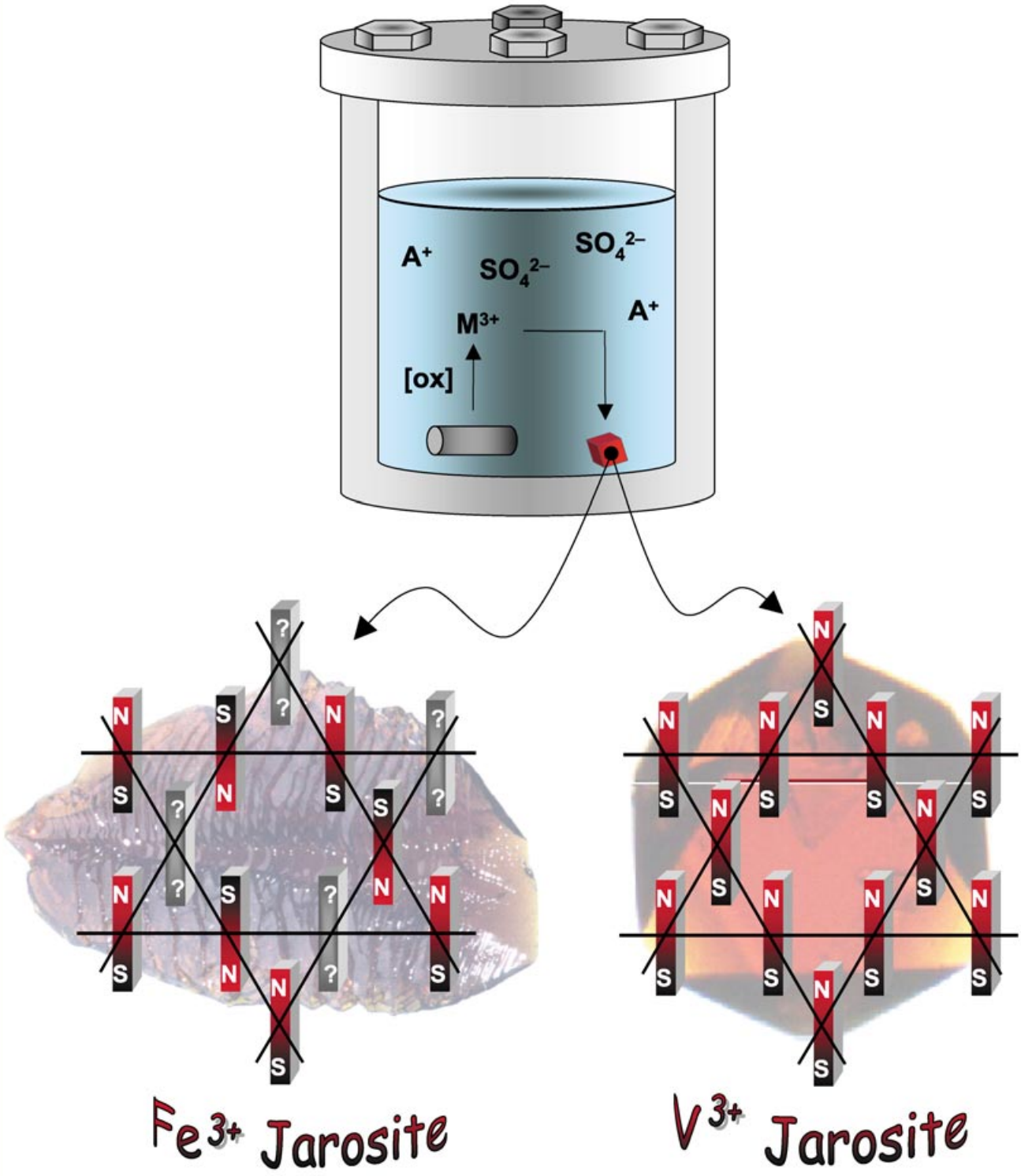

DOI: 10.1002/chem.200306074

Spin Frustration in 2D Kagomé Lattices: A Problem for Inorganic Synthetic Chemistry

Daniel G. Nocera,* Bart M. Bartlett, Daniel Grohol, Dimitris Papoutsakis, and Matthew P. Shores[a]

Abstract: A kagomé antiferromagnet presents an ideal construct for studying the unusual physics that result from the placement of magnetically frustrated spins on a low-dimensional lattice. Jarosites are the prototype for a spin-frustrated magnetic structure, because these materials are composed exclusively of kagomé layers. Notwithstanding, jarosite-type materials have escaped precise magnetic characterization over the past three decades, because they are notoriously difficult to prepare in pure and single-crystal forms. These hurdles have been overcome with the development of redox-based hydrothermal methods. Armed with pure and crystalline materials, several perplexing issues surrounding the magnetic properties of the jarosites have been resolved, yielding a detailed and comprehensive picture of the ground-state physics of this kagomé lattice.

Keywords: crystal growth · hydrothermal synthesis · jarosites · magnetic properties · redox chemistry · spin frustration

Introduction

The resonating liquid state, consisting of spin-singlet bonds, has been proposed to explain the scatterless hole transport in high T_c superconductors[1] and properties of other strongly correlated systems.[2,3] In this resonating valence bond (RVB) model, spins spontaneously pair into singlet bonds, which fluctuate between many different configurations. Central to the stability of such an RVB phase is geometric spin frustration, which produces a highly degenerate ground state owing to an exceptionally large number of different spin configurations at the same energy.[4] This situation allows for the intriguing possibility that quantum spin fluctuations are large enough to suppress long-range order, and therefore permit RVB to be established.[5,6]

The quantum-spin liquid phase that is a result of RVB is most likely to be found for magnetically frustrated spins on a low-dimensional lattice.[6] Of the various lattices that can support the RVB state, a Heisenberg antiferromagnet on a kagomé lattice emerges prominently.[7,8] Named after a form of a Japanese weave (kago = basket, mé = eye or hole), the kagomé lattice is composed of triangles that share corners to form two-dimensional sheets, shown in Figure 1. For classical spins with antiferromagnetic exchange, the ordered state shown in Figure 1 is but one of an infinite family of degenerate ground states. For quantum spins, the situation is

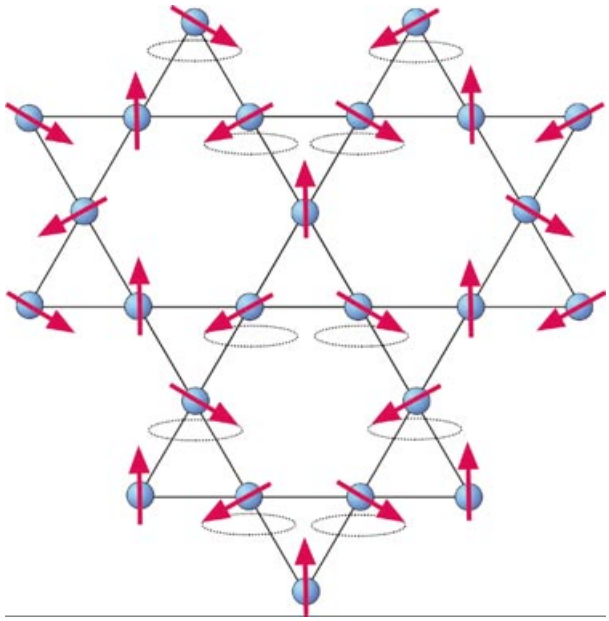

Figure 1. The kagomé lattice with spins in one possible ground-state configuration. Note that the spins on a hexagon can be rotated out of the plane about the dotted ellipse without changing the energy, thus giving rise to an infinite number of degenerate ground states.

[a] Prof. Dr. D. G. Nocera, B. M. Bartlett, Dr. D. Grohol, Dr. D. Papoutsakis, Dr. M. P. Shores
Department of Chemistry
Massachusetts Institute of Technology
77 Massachusetts Avenue
Cambridge, MA 02139-4307 (USA)
Fax: (+1) 617-253-7670
E-mail: nocera@mit.edu

 DOI: 10.1002/chem.200306074

even more complex; various theoretical treatments predict a ground state that remains quantum disordered at $T=0$.[9–11] The kagomé antiferromagnet therefore presents an ideal venue in which to look for both classical and quantum-spin liquid ground states, and more generally to study the strongly correlated electron problem.[12] In addition, the parallels highlighted in Scheme 1 suggest that the kagomé lattice is directly linked to the square lattice of rare-earth cuprates,

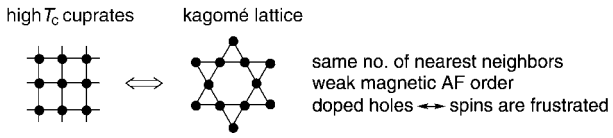

Scheme 1.

and to this end they can provide an incisive experimental guide to the development of theoretical models of high T_c superconductivity.

Despite intense interest in their magnetic ground states,[4,7–13] systematic investigation of kagomé lattices has been precluded by the paucity of materials. The layered garnets, $SrCr_xGa_{12-x}O_{19}$ (SCGO), have been investigated most intensively.[14–18] These materials contain an additional edge-sharing triangular (non-kagomé) lattice interposed between kagomé layers. The jarosite family of compounds, based on the $KFe_3(OH)_6(SO_4)_2$ parent, provides an alternative paradigmatic kagomé lattice, composed exclusively of kagomé layers formed from $Fe^{III}_3(\mu\text{-}OH)_3$ triangles (Figure 2a). These triangles are capped by sulfate anions positioned alternately up and down about a hexagonal network shown in Figure 2b.[19] The kagomé layers are separated by K^+ ions, which reside in the interlayer space in the same plane as the sulfur atoms of the capping tetrahedra (Figure 2c). An extensive family of jarosite compounds arises from the substitution of the Fe^{3+} ions by other M^{3+} ions (Cr^{3+}, Al^{3+}, Ga^{3+}, In^{3+}), and from the substitution of the K^+ on by other monovalent (Na^+, Rb^+, Ag^+, Tl^+, NH_4^+, H_3O^+) or divalent ($^1/_2Pb^{2+}$, $^1/_2Hg^{2+}$) ions; more members of the jarosite family result from the replacement of the sulfate group by either SeO_4^{2-} or CrO_4^{2-}.[19,20] The ability to systematically vary the intra- and interlayer metal ions, interlayer spacing, and the dimension of the intralayer triangles with the tetrahedral capping anion therefore presents jarosites as a unique framework in which to examine spin frustration.

Since the triangular spin arrangement of Figure 1 engenders an infinite number of degenerate ground states, jarosite materials should not display conventional long-range order (LRO).[4,13,21,22] Nevertheless, in all but one Fe^{3+} jarosite, LRO is observed. LRO may be established when the ground-state degeneracy created by spin frustration is lifted by the presence of further-neighbor exchange interactions, by anisotropy, or by lattice disorder. This last perturbation is particularly relevant to jarosites, because they have been notoriously difficult to prepare in pure forms. The monovalent A^+ ions are susceptible to replacement by hydronium ions and/or the coverage of the Fe^{3+} lattice sites is incomplete; consequently samples with magnetic site occupancies of 70–94% are obtained. The presence of site defects in strongly correlated magnetic arrays may significantly affect the compound's bulk behavior.[20,23] This is schematically represented in Figure 3, which shows that the frustration arising for anti-

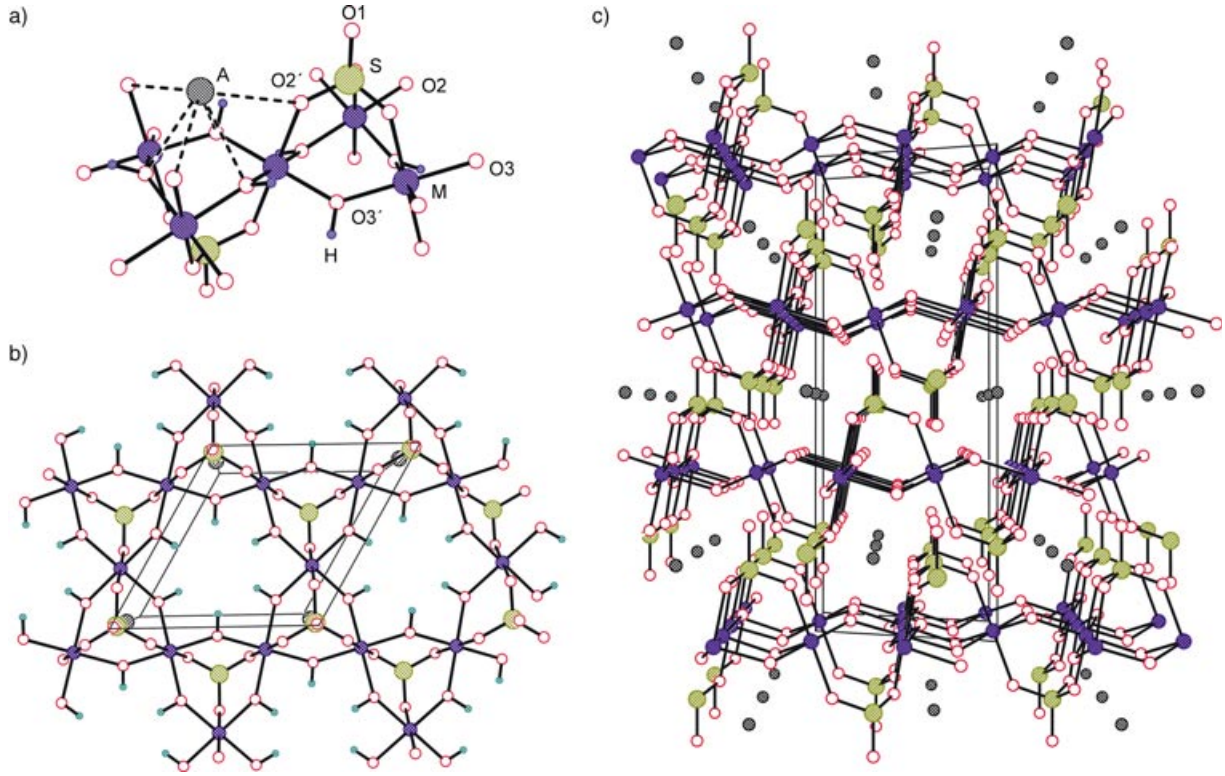

Figure 2. The X-ray crystal structure of a) the magnetic subunit of a triangular μ-hydroxy metal trimer, b) the in-plane segment of the kagomé layer, and c) side-on view of stacked kagomé layers. The sphere coding of the atoms is presented in a).

ferromagnetic spins is relaxed almost completely when magnetic site vacancies approach 30% that of a fully occupied lattice. Indeed, the presence of these vacancies has been most commonly cited as the reason for the observed LRO in jarosites. To further bolster this contention, hydronium jarosite, $(H_3O)Fe_3(OH)_6(SO_4)_2$, was the only jarosite known to possess nearly complete coverage (97%) of magnetic sites prior to our studies. The high magnetic site occupancy of this material is complemented by the absence of LRO[24–28] and the presence of spin-glass like behavior.[28,29]

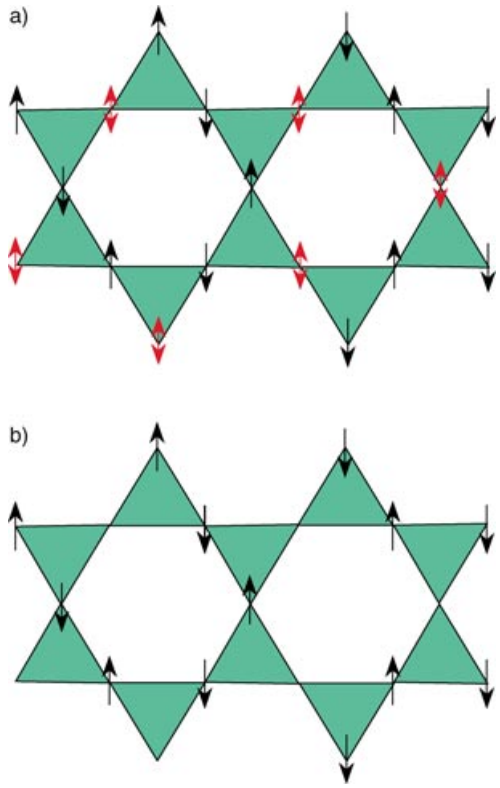

Figure 3. a) A segment of a kagomé lattice in which the magnetic sites are completely occupied. The red, double-headed arrows indicate spins that are frustrated on the kagomé lattice. b) The same segment of the kagomé lattice with 70% magnetic site occupancy. Note that there are no frustrated spins and the lattice is completely "relaxed".

The importance of jarosites as experimental models of the strongly correlated kagomé antiferromagnet problem, coupled to the ambiguities associated with their magnetic properties owing to the nonstoichiometric coverage of the magnetic lattice, provided an imperative to develop new synthetic routes that afford pure and crystalline jarosites. With such compounds in hand, a more comprehensive study of magnetism may be undertaken with the goals of 1) assessing whether LRO is an intrinsic property of the kagomé lattice of jarosites, 2) addressing the heretofore perplexing observation of the absence of LRO in the hydronium Fe^{3+} jarosite, and 3) correlating jarosite magnetism to d electron count and consequently the S value of the magnetic ion.

Synthesis of Pure Jarosites

The most common method of preparing Fe^{3+} jarosites is by precipitation under hydrothermal conditions (100–200 °C) according to reaction (1) of Table 1.[30,31] The drawback of this single-step reaction pathway is that the constituent ions, A^+, OH^-, M^{3+}, and SO_4^{2-} quickly precipitate; it is this fast precipitation that leads to jarosites with hydronium ions (H_3O^+) incorporated in the A^+ site and persistent deficiencies in the M^{3+} site occupancy.[32–34] Moreover, precipitation is so fast that crystallites larger than ~20 μm have not been obtained.[20,35,36]

In view of the issues highlighted in Figure 3, we sought new synthetic methods that would eliminate H_3O^+ site occupancy and M^{3+} site deficiency in jarosites. The redox-based hydrothermal methods listed in Table 1 have been developed to afford single crystalline and stoichiometrically pure (i.e., complete lattice coverage) jarosites containing the V^{3+}, Cr^{3+}, and Fe^{3+} magnetic ions of the formula, $AM_3(OH)_6(SO_4)_2$ ($A = Na^+$, K^+, Rb^+, Tl^+, and NH_4^+). For each of these reactions, control over the precipitation of the jarosite is achieved by using a redox reaction to slowly generate M^{3+} throughout the course of the hydrothermal process. Most of the redox methods rely on oxidation of metal or a low-valent ion to produce the M^{3+} species. The method schematically depicted in Figure 4 [reactions (2) and (3) in Table 1] conveniently relies on the use of protons as a primary oxidant. For the Cr^{3+} and V^{3+} jarosites, the M^{3+} ion is produced directly from the metal by its oxidation with the protons from the acidic reacting solution [reaction (2)].[37] The precipitation of the jarosite subsequently proceeds by reaction (1). The hydrothermal synthesis of Fe^{3+} jarosites possesses an additional step of control over the introduction of Fe^{3+} into solution.[38] Protons are of sufficient potential to only produce Fe^{2+} from Fe metal [reaction (3a)]; the Fe^{3+} is produced in a subsequent step by the reaction of Fe^{2+} with oxygen [reaction (3b)]. By simply controlling the oxygen partial pressure, the concentration of the oxygen in solution may be regulated with high fidelity. In this way, Fe^{3+} may be very slowly produced, thus affording large crystals with dimensions that are ten million times larger than those obtained by previously known techniques. Alternatively, Fe^{3+} can directly be produced from Fe metal (or Fe^{2+} ion) by ox-

Table 1. Redox-based hydrothermal methods developed for the synthesis of pure jarosites

$3M^{3+}+2A_2SO_4+6H_2O \rightarrow AM_3(OH)_6(SO_4)_2+3A^++6H^+$	(1)
oxidative hydrothermal methods	
$M+3H^+ \rightarrow M^{3+}+1.5H_2$ (M = V, Cr)	(2)
$Fe+2H^+ \rightarrow Fe^{2+}+H_2$	(3a)
$2Fe^{2+}+0.5O_2+2H^+ \rightarrow 2Fe^{3+}+H_2O$	(3b)
$3Fe+4.5A_2S_2O_8+6H_2O \rightarrow AFe_3(OH)_6(SO_4)_2+6H^++8A^++7SO_4^{2-}$	(4)
reductive hydrothermal methods	
$4VO^{2+}+2A_2SO_3+4H_2O \rightarrow AV_3(OH)_6(SO_4)_2+V^{3+}+2H^++3A^+$	(5)
$A^++4VO^{2+}+2(CH_3O)_2SO+8H_2O \rightarrow AV_3(OH)_6(SO_4)_2+V^{3+}+6H^++4CH_3OH$	(6)

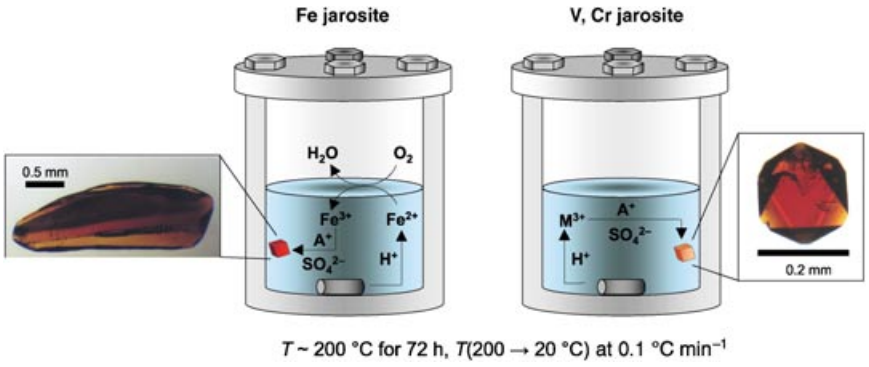

Figure 4. Redox-based hydrothermal synthesis of stoichiometrically pure, single crystalline iron (left) and vanadium and chromium (right) jarosites. The reaction is performed at pH = 1 to 1.5. Large single crystals of pure $KFe_3(OH)_6(SO_4)_2$ and $KV_3(OH)_6(SO_4)_2$ are shown.

idation with persulfate [reaction (4)]. In this process, the main constituent building blocks of the jarosite lattice, the Fe^{3+} and SO_4^{2-} ions, are both produced by the redox reaction.

The availability of convenient V^{4+} starting materials, coupled to the resiliency of V^{3+} to reduction, allows for V^{3+} jarosites to be prepared by reductive as well as oxidative hydrothermal methods. The V^{3+} ion may be slowly produced hydrothermally by reducing V^{4+} in the form of $VOCl_2$ with sulfite ion SO_3^{2-} [reaction (5)] under acidic conditions (pH ~1.5). Similar to reaction (3), the SO_4^{2-}-capping group, as well as the M^{3+} ion, are generated by the redox reaction. Alternatively, dimethylsulfite, $(CH_3O)_2SO$, is also a competent reductant of $VOCl_2$ under hydrothermal conditions at 200 °C [reaction (6)]. The hydrothermal reduction method leads to pure jarosites of high crystal quality, but of crystal size that is not significantly improved with respect to the oxidation approach presented in Figure 4.

Each of the redox-based synthetic methods listed in Table 1 yields $AM_3(OH)_6(SO_4)_2$ products that analyze at 100 ± 1.5 % in the M^{3+} ion, 100 ± 1.5 % in the A^+ ion, 99.5 ± 1.0 % in S, and 99.5 ± 3 % in H. All jarosites have been analyzed by single-crystal X-ray analysis, which reveals an isostructural intralayer for any M^{3+} ion or A^+ interlayer ion; only the spacing between the layers is varied by A^+ substitution. The structural rigidity of the kagomé lattice is highlighted in Table 2, which lists selected bond lengths and angles for a series of V^{3+}, Cr^{3+}, and Fe^{3+} jarosites for a given A^+ interlayer ion. This structural homology is powerful because we are assured that changes in magnetic properties of different jarosites are due to the intrinsic spin physics of the kagomé lattice and not due to trivial structural changes of the lattice (e.g., M-OH-M bond angle, M–M distance). Therefore, precise magneto-electronic correlations may be established among the various jarosite compounds.

Magnetism of Jarosites

Vanadium jarosites: The V^{3+} jarosites are not directly relevant to the strongly correlated electron problem, because the nearest neighbor interaction is ferromagnetic; thus the spins are not frustrated. Nevertheless, the materials are interesting in their own right.

A Curie–Weiss temperature $\Theta_{CW} \sim +53$ K establishes the presence of the ferromagnetic nearest-neighbor interaction of $NaV_3(OH)_6(SO_4)_2$, which is an archetype for the V^{3+} jarosite series.[39] Below critical temperature, $T_c = 33.3(1)$ K, the spins on the V^{3+} ions order ferromagnetically within each layer, and the layers stack antiferromagnetically. The consequences of this ordering are apparent from several experiments:[40]

1) Single-crystal magnetic susceptibility measurements display a pronounced anisotropy. Figure 5 displays the field-dependent behavior of the magnetization for a crystal with an external magnetic field applied (H_{appl}) parallel and perpendicular to the *c* axis, which is orthogonal to the kagomé layers. When the field is applied parallel

Table 2. Structural comparison of transition metal jarosites.

	V			Cr			Fe		
	Na^+	K^+	Rb^+	Na^+	K^+	Rb^+	Na^+	K^+	Rb^+
bond lengths [Å]									
S–O1	1.461(8)	1.461(11)	1.458(11)	1.459(6)	1.459(9)	1.44(2)	1.462(7)	1.460(7)	1.452(10)
S–O2	1.476(5)	1.471(6)	1.478(7)	1.481(4)	1.481(5)	1.47(1)	1.483(4)	1.481(4)	1.481(5)
M–O2	2.054(4)	2.063(5)	2.064(6)	1.994(3)	2.008(5)	2.016(9)	2.061(4)	2.066(4)	2.070(5)
M–O3	1.989(2)	1.991(2)	1.988(3)	1.969(2)	1.965(2)	1.996(4)	1.994(2)	1.987(2)	1.984(2)
M–M	3.643	3.627	3.640	–	–	–	3.671	3.652	3.657
A–O2	2.949(5)	2.975(6)	2.998(6)	2.913(4)	2.937(5)	2.975(9)	2.961(4)	2.971(4)	2.999(5)
A–O3	2.756(4)	2.851(5)	2.928(6)	2.710(4)	2.826(5)	2.902(9)	2.727(4)	2.826(4)	2.902(5)
bond angles [°]									
O2-M-O3	92.53(14)	92.40(19)	92.0(2)	92.3(1)	91.9(2)	91.3(3)	91.84(13)	91.77(13)	91.04(17)
O3-M-O3	90.9(3)	90.5(3)	91.0(4)	91.4(2)	90.0(3)	89.2(6)	91.8(3)	90.5(2)	90.1(3)
M-O3-M	132.6(2)	132.0(3)	132.5(3)	133.4(2)	133.5(3)	133.6(5)	134.0(2)	133.5(2)	134.4(3)
interlayer spacing									
d_{003} [Å]	16.851(2)	17.399(2)	17.835(7)	16.533(5)	17.165(2)	17.587(3)	16.605	17.185(2)	17.568(3)

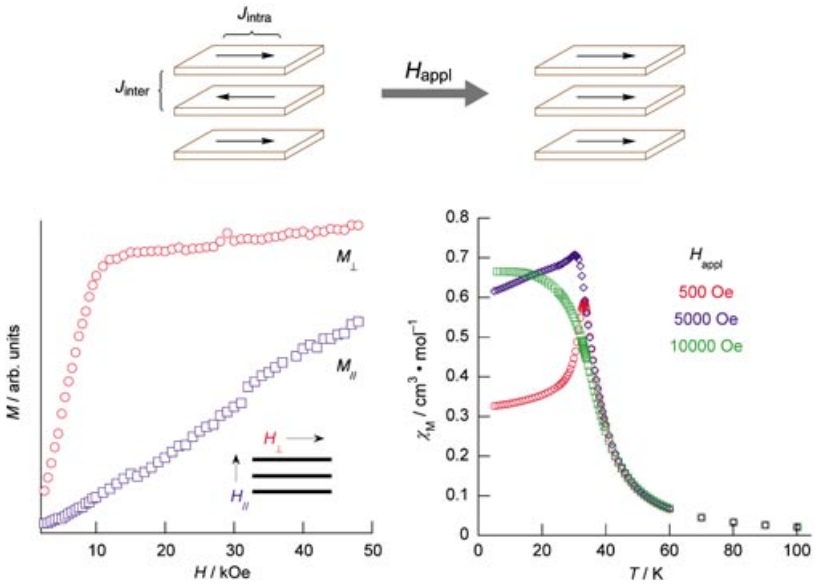

Figure 5. LRO in V^{3+} jarosites arises from the antiferromagnetic ordering of ferromagnetic kagome layers. Left panel: Magnetization versus H plot of a $NaV_3(OH)_6(SO_4)_2$ single crystal with an external field applied orthogonal (□, $M_\parallel$) and parallel (○, $M_\perp$) (and therefore orthogonal to the kagomé planes) to the c axis. Right panel: χ_M (per mole of vanadium) versus T plot of $NaV_3(OH)_6(SO_4)_2$ under different external fields (indicated in the figure: H_{appl}). Data for the V^{3+} jarosites with $A^+ = K^+$, Rb^+, NH_4^+, and Tl^+ are similar.

to the c axis (perpendicular to the layers), the magnetization within the layers, $M_\parallel$, increases linearly with field strength, but does not saturate at H_{appl} approaching 50 kOe. The V^{3+} single-ion anisotropy confines the exchange-coupled moments to lie within the kagomé plane, thereby hardening the out-of-plane motion. Conversely, when the field is applied orthogonal to the hard axis (perpendicular to the c axis, parallel to the kagomé layers), the magnetization, $M_\perp$, increases abruptly and attains a limiting value when H_{appl} is in excess of 10 kOe along the kagomé layers. As schematically indicated in Figure 5, this result is consistent with the external field overwhelming the coupling between layers.

2) Application of sufficiently strong H_{appl} eradicates the antiferromagnetic transition at T_c. As shown in Figure 5 for $NaV_3(OH)_6(SO_4)_2$, the sharp maximum at $T_c = 33.3$ K observed for $H_{appl} = 0.5$ kOe, is replaced by a broader peak centered at ~30.3 K when $H_{appl} = 5$ kOe; the maximum is completely suppressed when $H_{appl} \geq 10$ kOe. The critical field for this antiferromagnetic to paramagnetic transition is estimated to be 6 kOe.
3) T_c monotonically shifts to lower temperature as the size of the interlayer cation is increased. The results of Figure 6 are consistent with the attenuation in antiferromagnetic coupling between the layers as the distance between ferromagnetic sheets is increased.
4) Powder neutron diffraction measurements (Figure 7) show peaks that indicate a doubling of the c axis of the magnetic unit cell below T_c.[41] The {0,0,1.5} reflection is the most intense and appears precisely twice the interlayer spacing. These data are nicely fit by a model of antiferromagnetically stacked ferromagnetic layers; no evidence is seen for a spin component along the c axis.

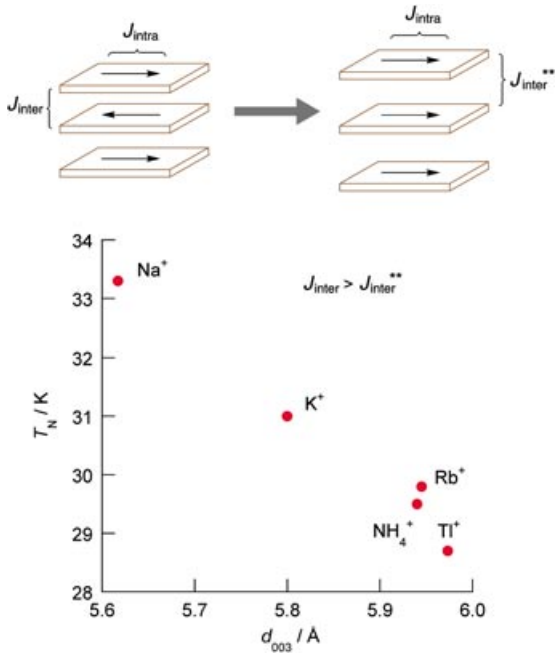

Figure 6. LRO in vanadium jarosites arises from antiferromagnetic stacking of ferromagnetic layers. The critical ordering temperature, T_c, decreases with increasing layer separation.

The V^{3+} jarosites are the first kagomé-based materials to display appreciable intralayer ferromagnetism. As a result of the coupling among V^{3+} ions within $V_3(OH)_6(SO_4)_2^-$ triangles, the V^{3+} jarosites display the unusual property for an inorganic compound of antiferromagnetically stacked ferromagnetic layers (sometimes referred to as metamagnetism).[42–44] The limits of this behavior can be addressed synthetically with the preparation of layered jarosites with expanded interlayer spacings. One clear line of synthetic inquiry follows the replacement of the sulfate capping group with that of phosphonate, RPO_3^{2-}, to form inorganic–organic hybrid structures. A phosphonate capping group will maintain the 2− charge of the sulfate cap of the native jarosites as well as the tripodal base of three oxygen atoms, which are needed to axially bind the V^{3+} ions of the intralayer triangle. Unlike sulfate, however, the interlayer spacing should be easily adjusted by varying the size of the apical R group.

Chromium jarosites: The Cr^{3+} jarosites are known to be antiferromagnetic and display a very low ordering temperature

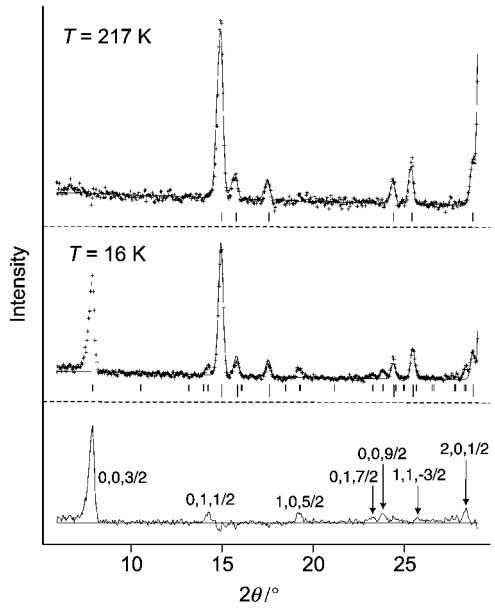

Figure 7. Comparison of powder neutron diffraction data for $NaV_3(OD)_6(SO_4)_2$, at 217 K (top), 16 K (middle), and magnetic peaks resulting from subtraction of the two sets of data (bottom). Allowed nuclear reflection positions are marked with longer vertical lines and allowed magnetic reflection positions are marked with shorter lines.

(~4 K).[45,46] However, these jarosites also suffer from the impurity and nonstoichiometry problems to perhaps an even larger extent than their Fe^{3+} counterparts. One in-depth neutron study published so far indicated the coverage of the Cr^{3+} ion to be 76%,[45] while another indicated a much higher occupancy of 95%,[46] and yet other studies failed to disclose the coverage at all.[47,48] To our knowledge, neither a stoichiometrically pure Cr^{3+} jarosite nor a single crystal has been prepared in the absence of the synthetic redox methods, which readily adapted to Cr^{3+} as described by reaction (2) of Table 1. Equipped with the new synthetic methodology, we have prepared single crystals of several Cr^{3+} jarosite representatives, acquired single-crystal X-ray data sets, and refined their structures. Important points that have emerged are that Cr^{3+} jarosites exhibits consistent Curie–Weiss temperatures of $\Theta_{CW} \sim -70$ K, regardless of the nature of the interlayer cation. In addition, as highlighted in Table 2, these materials are isostructural with their V^{3+} and Fe^{3+} counterparts. Accordingly, the nearest-neighbor antiferromagnetic exchange and resulting spin frustration are a direct consequence of the d^3 electron count of the magnetic Cr^{3+} ion.

Iron jarosites: The Fe^{3+} jarosites are strongly frustrated owing to a very pronounced intralayer antiferromagnetic exchange interaction ($\Theta_{CW} = -820 \pm 10$ K). We have performed detailed studies on the magnetism of the pure samples.[38] Our findings are as follows:

1) All stoichiometrically pure Fe^{3+} jarosites display LRO at finite temperatures.
2) The magnetic behavior of alkali metal ion members of the jarosite series is characterized by a prominent Néel transition at $T_N \sim 65$ K (see Figure 8 and Table 3), which is in accordance with the highest T_N values previously observed either by susceptibility or neutron diffraction measurements. The maximum is frequency-independent in the ac magnetic susceptibility plot, indicating the absence of spin-glass behavior.
3) Pure jarosite samples are further distinguished by the presence of weak ferromagnetism associated with a secondary transition temperature, T_D, at which the zero-field-cooled–field-cooled (ZFC-FC) magnetic susceptibility plots diverge and at which the onset of a remanent magnetization is observed (Figure 8).
4) Magnetic susceptibility measurements of large single crystals of $KFe_3(OH)_6(SO_4)_2$ oriented in the magnetic field along distinct axes (Figure 8) reveal anisotropic behavior in accordance with the expectation for a strongly frustrated spin system. LRO is associated with an out-of-plane spin component as indicated by the sharp maximum at $T_N \sim 65$ K for fields orthogonal to the kagomé planes. The results are consistent with LRO arising from spin anisotropy developed by the Dzyaloshinsky–Moriya (DM) interaction,[49] which causes spin canting within the layer as a result of the tilt of the FeO_6 octahedron (see Table 3).

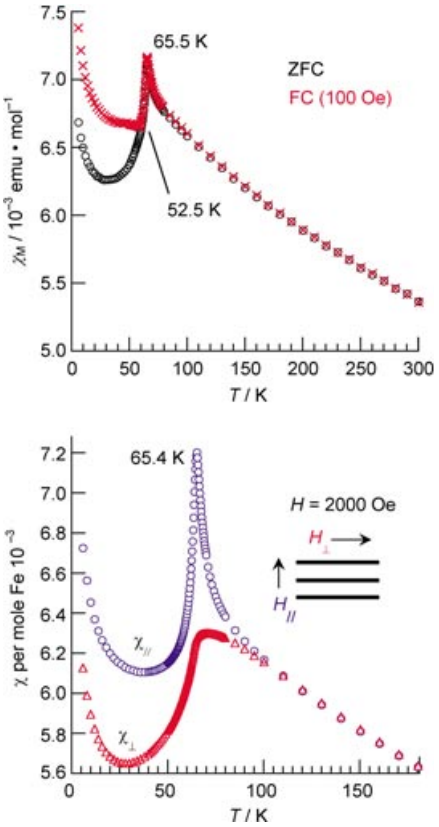

Figure 8. Magnetic susceptibility measurements of $KFe_3(OH)_6(SO_4)_2$. Top panel: The χ_M versus T plot of a powder measured under zero-field (○) and field-cooled (×) conditions ($H_m = H_c = 50$ Oe). Bottom panel: Magnetic susceptibility of an oriented single crystal with an external field applied parallel (○, $H_\perp$) and perpendicular (△, $H_\parallel$) (and therefore orthogonal to the kagomé planes) to the c axis.

Table 3. Magnetic properties of selected Fe^{3+} jarosites

Cation	T_N [K]	Θ_{CW} [K]	d_{003} [Å]	FeO_6 tilt angle [°]	Fe-O-Fe [°]
K^+	65.4	−828	5.728(2)	17.4(3)	133.6(2)
Rb^+	64.5	−829	5.856(3)	17.5(3)	134.4(3)
Tl^+	63.4	−838	5.870(2)	17.6(4)	134.4(4)
Na^+	61.5	−825	5.535(10)	17.6(3)	134.0(2)
Ag^+	59.5	−798	5.498(3)	17.9(3)	134.0(3)
$0.5\,Pb^{2+}$	56.4	−818	5.598(3)	17.7(3)	134.1(3)

5) The canted spin structure gives rise to a weak ferromagnetic component that is orthogonal to the kagomé layers. The observed cusp at T_N for Fe^{3+} jarosites establishes that this weak ferromagnet component couples antiferromagnetically between layers. Similar to the situation for V^{3+} jarosites, this antiferromagnetic exchange between layers can be overwhelmed with the application of sufficiently strong field; however, in the case of Fe^{3+} jarosites, a jump in the magnetization at a critical field, H_c, occurs when a magnetic field approaching 14 kOe is applied normal to the kagomé layers.[50] As schematically depicted in Scheme 2, this jump in magnetization is due to the alignment of canted spins between layers.

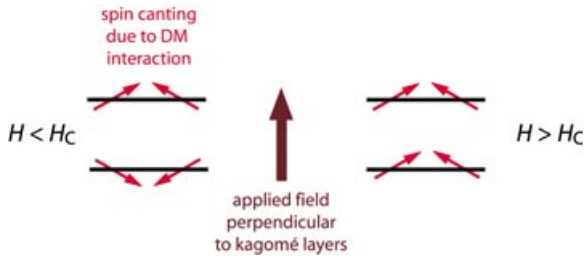

Scheme 2.

6) Single crystals of sufficient dimensions have enabled inelastic neutron diffraction scattering to be undertaken for the study of spin-waves of the 2D kagomé lattice.[51] For the first time in a geometrically frustrated spin system, a weakly dispersive zero-energy mode has been found.

Hydronium iron jarosite: The foregoing results establish that spin-frustrated jarosites exhibit LRO, even when the magnetic sites of the kagomé lattice are completely occupied. Then why is LRO absent in hydronium jarosite? The answer to this question may be found by consideration of the intrinsic reaction chemistry of hydronium jarosite. The hydroxyl groups of the intralayer $M^{III}{}_3(\mu\text{-}OH)_3$ triangles are in the immediate vicinity of each intralayer hydronium ion. Taken together with the large thermodynamic driving force for the acid–base reaction between H_3O^+ and OH^-, proton transfer from the interlayer hydronium ion to the bridging hydroxyls is favored [reaction (7)].

$$(H_3O)Fe_3(OH)_6(SO_4)_2 \rightarrow (H_3O)_{1-x}(H_2O)_xFe_3(OH)_{6-x}(H_2O)_x(SO_4)_2 \quad (7)$$

Direct evidence for this proton transfer comes from infrared spectra, which exhibit an absorption corresponding to the H-O-H bending mode of the H_2O molecule.[38] In stoichiometrically pure jarosites, water is absent in the lattice and consequently this absorption is not observed. In addition, the absorption of the O–H stretching vibration in the 3300–3400 cm^{-1} region is reduced in intensity and width. A second source of water in the jarosite lattice arises from the maintenance of charge balance within a kagomé lattice possessing M^{3+} site vacancies.[38] Protonation of OH^- by H^+ to form H_2O [reaction (8)] will prevent the accrual of negative charge on kagomé layers possessing M^{3+} site vacancies.

$$AFe_3(OH)_6(SO_4)_2 + 3x\,H^+ \rightarrow AFe_{3-x}(OH_2)_{3x}(OH)_{6-3x}(SO_4)_2 + x\,Fe^{3+} \quad (8)$$

Both the intrinsic and extrinsic proton transfer mechanisms described by reactions (7) and (8), respectively, prevail for the hydronium ion jarosite and more generally for any A^+ jarosite prepared by non-redox precipitation methods.

Proton-transfer reactions (7) and (8) have significant implications to the magnetism of jarosites, particularly as they pertain to LRO. Firstly, proton transfer will influence the primary intralayer exchange pathway. A significant decrease in the strength of magnetic exchange between metal centers accompanies the protonation of oxo-bridged bimetallic centers.[52,53] In view of the foregoing model in which intralayer exchange drives 3D ordering, protonation of the hydroxyl group mediating the nearest neighbor magnetic exchange will inevitably lead to a decrease in nearest neighbor exchange and consequently to depressed T_Ns in Fe^{3+} jarosites. Secondly, proton transfer will be a disordered chemical event in the jarosite lattice. Inasmuch as structural disorder is capable of inducing spin-glass behavior,[54,55] the spin-glass like properties of $(H_3O)Fe_3(OH)_6(SO_4)_2$ are due to structural and attendant magnetic disorder caused by proton-transfer reactions (7) and (8).

Magneto-Electronic Correlation in Jarosites

The magnetic M^{3+} ions of jarosites reside in a tetragonally distorted crystal field. Axial elongation of the M^{3+} octahedron lifts the degeneracy of the t_{2g} and e_g orbital sets in a parent octahedral field: the t_{2g} orbital set splits into a lower energy, doubly degenerate $e_g(d_{xz},d_{yz})$ orbital set and a singly degenerate $b_{2g}(d_{xy})$ orbital; the e_g orbital set splits into a lower energy $a_{1g}(d_{z^2})$ orbital and higher energy $b_{1g}(d_{x^2-y^2})$ orbital.

Figure 9 presents the magnetic properties of the known first-row transition-metal jarosites together with the d electron occupancy of the crystal field energy level diagram. The two d electrons of V^{3+} jarosite occupy the $e_g(d_{xz},d_{yz})$ orbital. The positive Θ_{CW} of V^{3+} jarosite reveals that the π symmetry pathway, composed of the interaction of the $e_g(d_{xz},d_{yz})$ orbital set with the p orbital of the bridging hydroxide, leads to a ferromagnetic exchange interaction. Neutron diffraction studies show that the O–H bond is rotated 18° out of the Fe-O-Fe plane. Our experiments show that

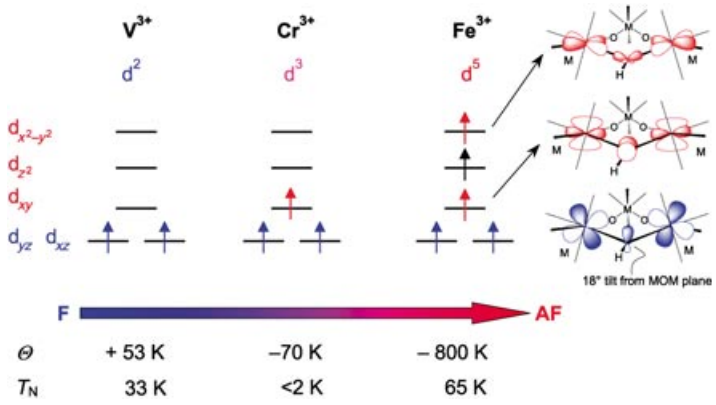

Figure 9. The correlation between magnetic properties of jarosites and the d orbital occupancy of the M^{3+} ion in the tetragonal crystal field. The superexchange pathway composed of each of the d orbitals is pictorially depicted.

this rotation is apparently sufficient to decouple the dπ orbitals of neighboring V^{3+} metals to lead to a ferromagnetic ground state. This is not so for Cr^{3+} jarosite; the sign of the nearest-neighbor magnetic coupling changes upon the addition of one more electron to the crystal field diagram. Occupation of the metal d_{xy} orbitals in Cr^{3+} jarosites leads to a dominant antiferromagnetic exchange term through a $d_{xy}(\sigma)$–p(O)–$d_{xy}(\sigma)$ pathway that is capable of overwhelming the ferromagnetic contribution of the $d_{xz}(\pi)$–p(O)–$d_{xz}(\pi)$ pathway. Placement of two more electrons in the d_{z^2} and $d_{x^2-y^2}$ orbitals of Fe^{3+} jarosite increases this antiferromagnetic exchange interaction within the kagomé lattice by more than an order of magnitude. Inasmuch as the overlap between the d_{z^2} orbitals and the p orbitals of the bridging hydroxide is small, it is the overlap of the $d_{x^2-y^2}$ orbitals with the μ-hydroxy p orbital that carries the large antiferromagnetic exchange interaction of Fe^{3+} jarosites. The observed properties of this exchange pathway concur with long-standing predictions of Goodenough and Kanamori,[56,57] and accounts for the high degree of spin frustration observed in the d^5 ($S=5/2$) spin jarosite system.

Conclusions and Outlook

Spin-frustrated kagomé lattices of jarosite compounds exhibit LRO. This result is sufficiently daunting to seemingly banish jarosites from the roster of materials that exhibit disordered ground states. But the new results described herein only present immediate challenges to realizing a spin liquid ground state—challenges that can be overcome with the application of the craft of inorganic synthesis.

Spin anisotropy arising from the Dzyaloshinsky–Moriya (DM) interaction provides a mechanism for LRO in jarosites. A roadmap exists to the preparation of jarosite materials with suppressed DM interactions. The DM interaction is given by Equation (9):[49]

$$\mathbf{D}_{ij} \cdot (\mathbf{S}_i \times \mathbf{S}_j) \qquad (9)$$

in which $\mathbf{D}_{ij}$ is the DM vector and $(\mathbf{S}_i \times \mathbf{S}_j)$ is the cross product term of adjacent spins within the layer. In the kagomé lattice, $(\mathbf{S}_i \times \mathbf{S}_j)$ is nonzero for adjacent spins owing to a tilting of FeO_6 octahedra (17° as measured from crystal structures, see Table 3); this tilting leads to the corrugation of the kagomé layers observed in Figure 2c. The FeO_6 tilt angle is determined by the size of the capping group as it is the three oxygens from the pyramidal base of the TO_4^{2-} cap that occupy the axial coordination sites of the FeO_6 tetragonally distorted octahedron. Accordingly, the kagomé layers of jarosite may be flattened by increasing the dimension of the pyramidal base of the TO_4^{2-} capping group. For such materials, the DM interaction should be reduced, and correspondingly, LRO should be attenuated as this tilt angle approaches zero (i.e. $\mathbf{S}_i \times \mathbf{S}_j = 0$).

Alternatively, the continued development of hydrothermal methods that afford large single crystals may permit the spin liquid properties to be investigated with current jarosite materials. Heat capacity measurements on Fe^{3+} jarosite show a significant loss of entropy (from that expected for $S=5/2$) at temperatures above T_N.[50] This result implies a short-range correlation of spins in the kagomé plane above the ordering temperature. Such short-range order should be revealed by the inelastic neutron scattering technique. Along these lines, the Cr^{3+} jarosite system, with its very low ordering temperature, appears to be particularly well-suited for uncovering short-range properties as T_N is approached. However, large single crystals of this material need to be synthesized.

Finally, many theoretical investigations predict that the elusive RVB spin liquid ground state is most likely to be found in an $S=1/2$ kagomé antiferromagnet.[7,8,12,22] However, such a compound has yet to be synthesized. The Ti^{3+} ion carries the proper charge for the jarosite framework and it is an $S=1/2$ ion, but the system confronts two hurdles. The Ti^{3+} ion is extremely unstable with respect to oxidation to produce Ti^{4+}, especially when titanium is in an oxygen-rich environment, as is the case for the jarosite lattice. Consequently, a Ti^{3+} jarosite will be difficult to prepare in pure form. Even if this hurdle is surmounted, the Ti^{3+} jarosite will most likely be a kagomé ferromagnet. The single electron of a Ti^{3+} ion will reside in the same $e_g(d_{xz},d_{yz})$ orbital set that is shown in Figure 9 for V^{3+} jarosite. As already established in the context of V^{3+} jarosite magnetism, the dπ–p(O)–dπ pathway in the $M^{III}_3(\mu\text{-}OH)_3$ triangles support a nearest-neighbor ferromagnetic exchange interaction and not the antiferromagnetic one required for spin frustration. Continuing within the framework of Figure 9, a $d_{x^2-y^2}$ orbital occupancy engenders the strongest antiferromagnetic exchange interaction. Coupling the requirement of $d_{x^2-y^2}$ orbital occupancy to that of an $S=1/2$ spin state identifies a singular synthetic target—a jarosite with Cu^{2+} as the magnetic ion. In such a material, a 4+ interlayer cation is required to maintain charge neutrality, that is, $A^{IV}M^{II}_3(OH)_6(SO_4)_2$. Recently, Rao and co-workers have employed the polyammonium 4+ ion, triethylenetetraammonium ($[H_4TETA]^{4+}$) to stabilize an all Fe^{2+} analogue of jarosite, $[H_4TETA][Fe^{II}_3F_6(SO_4)_2]$.[58] The structure features an $[Fe_3F_6]$ kagomé-like lattice capped by sulfate anions and hydrogen bonded to the charge-balancing TETA cation. Though the two-dimensional lattice is distorted and therefore not ideal for studying spin

frustration,[59] the new synthetic methods presage the stabilization of a M^{2+} ion such as Cu^{2+} in the jarosite-type lattice.

[1] P. W. Anderson, *Science* **1987**, *235*, 1196–1198.
[2] G. Baskaran, Z. Zou, P. W. Anderson, *Solid State Commun.* **1987**, *63*, 973–976.
[3] K. Ueda, H. Kontani, M. Sigrist, P. A. Lee, *Phys. Rev. Lett.* **1996**, *76*, 1932–1935.
[4] A. P. Ramirez, *Annu. Rev. Mater. Sci.* **1994**, *24*, 453–480.
[5] R. Coldea, D. A. Tennant, Z. Tylczynski, *Phys. Rev. B* **2003**, 68, 134424/1–16.
[6] T. Koretsune, M. Ogata, *Phys. Rev. Lett.* **2002**, *89*, 116401/1–4.
[7] C. Waldtmann, H. U. Everts, B. Bernu, C. Lhuillier, P. Sindzingre, P. Lecheminant, L. Pierre, *Eur. Phys. J. B* **1998**, *2*, 501–507.
[8] M. B. Hastings, *Phys. Rev. B* **2001**, *63*, 014413/1–16.
[9] A. B. Harris, C. Kallin, A. J. Berlinsky, *Phys. Rev. B* **1992**, *45*, 2899–2919.
[10] J. T. Chalker, J. F. G. Eastmond, *Phys. Rev. B* **1992**, *46*, 14201–14204.
[11] S. Sindzingre, G. Misguich, C. Lhuillier, B. Bernu, L. Pierre, C. Waldtmann, H. U. Everts, *Phys. Rev. Lett.* **2000**, *84*, 2953–2956.
[12] C. Lhuillier, Claire, G. Misguich, Gregoire, *Lect. Notes Phys.* **2001**, *595*, 161–190.
[13] E. F. Shender, P. C. W. Holdsworth in *Fluctuations and Order*, (Ed.: M. Millonas), Springer, Berlin, **1996**, p. 259.
[14] S. H. Lee, C. Broholm, G. Aeppli, T. G. Perring, B. Hessen, A. Taylor, *Phys. Rev. Lett.* **1996**, *76*, 4424–4427.
[15] C. Broholm, G. Aeppli, G. P. Espinosa, A. S. Cooper, *Phys. Rev. Lett.* **1990**, *65*, 3173–3176.
[16] A. P. Ramirez, G. P. Espinosa, A. S. Cooper, *Phys. Rev. Lett.* **1990**, *64*, 2070–2073.
[17] A. Keren, P. Mendels, M. Horvatic, F. Ferrer, Y. J. Uemura, M. Mekata, T. Asano, *Phys. Rev. B* **1998**, *57*, 10745–10749.
[18] A. Keren, Y. J. Uemura, G. Luke, P. Mendels, M. Mekata, T. Asano, *Phys. Rev. Lett.* **2000**, *84*, 3450–3453.
[19] J. L. Jambor, *Can. Mineral.* **1999**, *37*, 1323–1341.
[20] A. S. Wills, A. Harrison, *J. Chem. Soc. Faraday Trans.* **1996**, *92*, 2161–2166.
[21] J. N. Reimers, A. J. Berlinsky, *Phys. Rev. B* **1993**, *48*, 9539–9554.
[22] J. T. Chalker, P. C. W. Holdsworth, E. F. Shender, *Phys. Rev. Lett.* **1992**, *68*, 855–858.
[23] A. S. Wills, A. Harrison, C. Ritter, R. I. Smith, *Phys. Rev. B* **2000**, *61*, 6156–6169.
[24] A. S. Wills, V. Dupuis, E. Vincent, J. Hammann, R. Calemczuk, *Phys. Rev. B* **2000**, *62*, R9264–R9267.
[25] A. Harrison, K. M. Kojima, A. S. Wills, Y. Fudamato, M. I. Larkin, G. M. Luke, B. Nachumi, Y. J. Uemura, D. Visser, J. S. Lord, *Physica B* **2000**, *289–290*, 217–220.
[26] G. S. Oakley, S. Pouget, A. Harrison, J. Frunzke, D. Visser, *Physica B* **1999**, *267–268*, 145–148.
[27] G. S. Oakley, D. Visser, J. Frunzke, K. H. Andersen, A. S. Wills, A. Harrison, *Physica B* **1999**, *267–268*, 142–144.
[28] A. S. Wills, A. Harrison, S. A. M. Mentink, T. E. Mason, Z. Tun, *Europhys. Lett.* **1998**, *42*, 325–330.
[29] T. Inami, M. Nishiyama, S. Maegawa, Y. Oka, *Phys. Rev. B* **2000**, *61*, 12181–12186.
[30] J. E. Dutrizac, *Metall. Trans. B* **1983**, *14*, 531–539.
[31] J. E. Dutrizac, S. Kaiman, *Can. Mineral.* **1976**, *14*, 151–158.
[32] J. E. Dutrizac, T. T. Chen, *Can. Mineral.* **2003**, *41*, 479–488.
[33] J. Kubisz, *Mineral. Pol.* **1970**, *1*, 47–59.
[34] J. Kubisz, *Mineral. Pol.* **1971**, *2*, 51–60.
[35] J. L. Jambor, J. E. Dutrizac, *Can. Mineral.* **1985**, *23*, 47–51.
[36] A. S. Wills, A. Harrison, C. Ritter, R. I. Smith, *Phys. Rev. B.* **2000**, *61*, 6156–6169.
[37] D. Grohol, D. G. Nocera, *J. Am. Chem. Soc.* **2002**, *124*, 2640–2646.
[38] D. Grohol, D. G. Nocera, D. Papoutsakis, *Phys. Rev. B* **2003**, *67*, 064401/1–13.
[39] D. Grohol, D. Papoutsakis, D. G. Nocera, *Angew. Chem.* **2001**, *113*, 1567–1569; Angew. *Chem. Int. Ed.* **2001**, *40*, 1519–1521.
[40] D. Papoutsakis, D. Grohol, D. G. Nocera, *J. Am. Chem. Soc.* **2002**, *124*, 2647–2656.
[41] D. Grohol, Q. Z. Huang, B. H. Toby, J. W. Lynn, Y. S. Lee, D. G. Nocera, *Phys. Rev. B* **2003**, *68*, 094404/1–7.
[42] L. J. de Jongh in *Physics and Chemistry of Materials with Low-Dimensional Structures, Vol. 9*, (Ed.: F. Levy), Kluwer, Dordrecht, The Netherlands, **1990**.
[43] D. G. Rancourt, I. A. D. Christie, G. Lamarche, I. Swainson, S. Flandrois, *J. Magn. Magn. Mater.* **1994**, *138*, 31–44.
[44] K. Awaga, E. Coronado, M. Drillon, *Mater. Res. Soc. Bull.* **2000**, *25*, 52–59.
[45] S.-H. Lee, C. Broholm, M. F. Collins, L. Heller, A. P. Ramirez, C. Kloc, E. Bucher, R. W. Erwin, N. Lacevic, *Phys. Rev. B* **1997**, *56*, 8091–8097.
[46] T. Inami, T. Morimoto, N. Nishiyama, S. Maegawa, Y. Oka, H. Okumura, *Phys. Rev. B* **2001**, *64*, 054421/1–6.
[47] M. Nishiyama, T. Morimoto, S. Maegawa, T. Inami, Y. Oka, *Can. J. Phys.* **2001**, *79*, 1511–1516.
[48] T. Morimoto, M. Nishiyama, S. Maegawa, Y. Oka, *J. Phys. Soc. Jpn.* **2003**, *72*, 2085–2090.
[49] M. Elhajal, B. Canals, C. Lacroix, *Phys. Rev. B* **2002**, *66*, 014422/1–6.
[50] D. Grohol, K. Matan, Y. S. Lee, D. G. Nocera, unpuiblished results.
[51] K. Matan, D. Grohol, Y. S. Lee, D. G. Nocera, unpublished results.
[52] D. M. Kurtz, *Chem. Rev.* **1990**, *90*, 585–606.
[53] O. Kahn in *Molecular Magnetism*, VCH, Weinheim, **1993**.
[54] K. Binder, A. P. Young, *Rev. Mod. Phys.* **1986**, *58*, 801–976.
[55] J. A. Mydosh in *Spin Glasses: An Experimental Introduction*, Taylor and Francis, London, **1993**.
[56] J. B. Goodenough, *Phys. Chem. Solids* **1958**, *6*, 287–297.
[57] J. Kanamori, *Phys. Chem. Solids* **1959**, *10*, 87–98.
[58] G. Paul, A. Choudhury , C. N. R. Rao, *Chem. Commun.* **2002**, 1904–1905.
[59] C. N. R. Rao, G. Paul, A. Choudhury, E. V. Sampathkumaran, A. K. Raychaudhuri, S. Ramasesha, I. Rudra, *Phys. Rev. B* **2003**, *67*, 134425/1–5.

Published online: May 26, 2004

